



## OPEN Effect of pH on niacinamide skin permeation

Thomas Sjöberg<sup>1,2</sup>, Silvia Letasiova<sup>3</sup>, Skaidre Jankovskaja<sup>1,2</sup>, Nina Hrapovic<sup>4</sup>, Christina Österlund<sup>4</sup>, Emelie Nilsson<sup>1,2</sup>, Johan Engblom<sup>1,2</sup>, Peter Spégel<sup>5</sup> & Sebastian Björklund<sup>1,2</sup>✉

Niacinamide (NIA) is a widely used skincare ingredient with established benefits for skin barrier support, inflammation reduction, and dermal health. However, the mechanisms governing its transdermal delivery remain insufficiently understood, particularly regarding how formulation pH influences its permeation through the stratum corneum (SC). This study investigates how donor phase pH (5.0 vs. 7.4) modulates NIA skin permeation and how these effects relate to pH induced changes in SC electrical properties. Franz cell diffusion experiments were combined with electrical impedance spectroscopy (EIS) using full-thickness human skin and 3D reconstructed epidermal tissue models. Permeation was quantified over 24 h and in pH switch experiments, while EIS characterized pH dependent changes in membrane resistance ( $R_{\text{mem}}$ ) and effective capacitance ( $C_{\text{eff}}$ ). Additional analyses assessed microbial conversion of NIA to nicotinic acid during prolonged exposure. Neutral donor pH (7.4) increased NIA permeation by roughly twofold compared with acidic pH (5.0) in both membrane types. Correspondingly, pH 7.4 decreased  $R_{\text{mem}}$  and increased  $C_{\text{eff}}$ , indicating pH driven changes in SC lipid organization and dielectric behavior. These effects were reversible and likely stem from alterations in SC lipid domains, including pH dependent partial deprotonation of free fatty acids that modifies the continuous lipid regions and introduce localized structural microdefects. Such changes enhance NIA and ion permeability and increase SC dielectric properties at neutral pH. Although microbial conversion of NIA to nicotinic acid was negligible within the first 24 h, it became clearly detectable upon prolonged experiments. In conclusion, donor phase pH is a critical determinant of NIA skin permeation, primarily through reversible modulation of SC lipid structure and transport pathways. These findings highlight the importance of pH control in topical formulations and underscore the need to consider microbiota-mediated transformations when evaluating the efficacy and safety of skin care products containing NIA.

**Keywords** Skin barrier, 3D reconstructed epidermis, Transdermal permeation pathways, Electrical impedance spectroscopy, Niacinamide conversion, Nicotinic acid

The skin barrier function is primarily regulated by the outermost layer of the epidermis, the stratum corneum (SC). This composite membrane, composed of non-viable keratinized cells (corneocytes) embedded in a continuous lipid matrix, resembles a brick-and-mortar structure<sup>1</sup>. The SC protects against harmful substances and minimizes transepidermal water loss (TEWL)<sup>2</sup>, functions largely attributed to its multilamellar lipid matrix<sup>3,4</sup>. Structural integrity of the SC is essential for skin health. In daily life, exposure to low relative humidity (RH) can lead to dry skin and impaired barrier function. Continuous hydration of the SC, maintained by the water gradient between underlying tissues and the external environment, is therefore critical for homeostasis. When the barrier is compromised, topical formulations containing small polar substances are commonly used to restore integrity.

Among these substances, niacinamide (NIA), also known as nicotinamide, has numerous applications in dermatology and skincare due to its positive effects on skin health<sup>5</sup>. NIA has been shown to reduce TEWL and improve skin pliability in clinical studies<sup>6–9</sup>. Recent findings indicate that NIA induces swelling between keratin monomers at low humidity (60% RH) without increasing overall SC water content, suggesting a plasticizing effect that enhances flexibility under dry conditions<sup>10</sup>. Despite being non-hygroscopic, NIA promotes water uptake in SC at high humidity (95% RH)<sup>10</sup>. Additionally, NIA exhibits anti-inflammatory properties, aiding in the management of acne, rosacea, and atopic dermatitis<sup>5,11</sup>. It also demonstrates antioxidant activity and may

<sup>1</sup>Department of Biomedical Science, Malmö University, Malmö, Sweden. <sup>2</sup>Biofilms Research Centre for Biointerfaces, Malmö University, Malmö, Sweden. <sup>3</sup>MatTek In Vitro Life Science Laboratories, Bratislava, Slovakia. <sup>4</sup>Global Research & Development, Oriflame Cosmetics AB, Stockholm, Sweden. <sup>5</sup>Department of Chemistry, Centre for Analysis and Synthesis, Lund University, Lund, Sweden. ✉email: sebastian.bjorklund@mau.se

reduce DNA damage from external stressors<sup>5,12,13</sup>. Clinical studies further report that creams containing NIA reduce wrinkles, fine lines, and skin surface roughness<sup>14–17</sup>. These findings suggest that NIA can influence both the molecular structure of the SC and biochemical processes in underlying viable cells. For the latter to occur, NIA must penetrate the SC barrier to reach viable cells of the skin tissue.

Transdermal delivery of NIA has been the subject of various studies aimed at enhancing its skin permeation. Despite its small molecular size (MW 122 g mol<sup>-1</sup>), the relatively hydrophilic nature of NIA (logD = 0.41 at pH 5.0 and logD = 0.39 at pH 7.4, estimated using Chemicalize, ChemAxon) limits its ability to partition into the multilamellar lipid matrix of the SC, making efficient transdermal delivery of NIA challenging. To improve dermal delivery of NIA, strategies such as using solvents with skin penetration enhancement properties have been explored in permeation studies with excised skin membranes. Solvents tested include glycerol, propylene glycol, dimethyl isosorbide, low-molecular-weight polyethylene glycols and alcohols. Among these, t-butyl alcohol, dimethyl isosorbide, and transcitol showed the most promising enhancement of NIA skin permeation<sup>18,19</sup>. NIA permeation has also been investigated using mixtures of propylene glycol, propylene glycol monolaurate, and isopropyl myristate, with combinations of propylene glycol and propylene glycol monolaurate showing notable enhancement of NIA delivery<sup>20</sup>.

In addition to solvents with penetration enhancing properties, pH may also influence NIA permeation, but this aspect has been far less explored. Previous studies examined the effect of receptor chamber pH (5.4 vs. 7.4) on NIA permeation<sup>21,22</sup>. However, these studies primarily aimed to optimize in vitro permeation protocols, including improving reproducibility and evaluating artificial membranes as substitutes for skin, and they reported no significant impact of receptor pH<sup>21,22</sup>. This is not surprising, as receptor pH mainly affects permeant solubility, and the solubility of NIA is not expected to vary within these pH ranges. In contrast, the barrier properties of the SC are expected to be influenced by the pH of the donor phase facing the skin surface. To our knowledge, no study has specifically examined how donor phase pH affects SC barrier properties in relation to NIA, including drug partitioning and diffusion characteristics.

In healthy individuals, the SC exhibits a mildly acidic pH of approximately 4.5–5.0, commonly referred to as the “acid mantle”<sup>23</sup>. This acidity is maintained by innate biochemical mechanisms and plays an essential role in barrier homeostasis<sup>23</sup>. In addition to biochemical regulation, physicochemical factors such as skin hydration and CO<sub>2</sub> gradients across the SC have also been proposed to influence the formation and maintenance of the pH<sup>24</sup>. The inherent pH gradient across the SC is a critical determinant of barrier function and can be substantially modified by topical formulations. Active alteration of SC surface pH, for example by application of topical products, represents a direct mechanism for influencing molecular transport across the SC. This effect can be rationalized by pH driven changes in the organization and mobility of SC lipids and proteins, which in turn can significantly affect SC permeability<sup>25–27</sup>.

In this study, we investigate how pH gradients influence NIA permeation across the SC using Franz cell diffusion experiments coupled with electrical impedance spectroscopy (EIS). EIS is a non-destructive technique that characterizes skin barrier electrical properties, including membrane resistance ( $R_{mem}$ ) and effective capacitance ( $C_{eff}$ ), which reflects passive ion transport and dielectric properties of the skin barrier, respectively<sup>28,29</sup>. This combined approach provides mechanistic insight into how pH modulates NIA transport. To broaden our analysis, we examined both full-thickness human skin and 3D reconstructed epidermal tissue models (EpiDerm). Human skin serves as the gold standard due to its native lipid and protein organization, though availability and donor variability pose limitations. EpiDerm provides a standardized alternative that reproduces key SC structural and functional features but lacks a dermal compartment and skin appendages. Comparing these membranes under controlled pH gradients allows us to assess the consistency of pH dependent effects on NIA permeation and electrical properties, supporting the use of reconstructed skin tissue models for regulatory and research applications.

## Materials and methods

### Materials

Niacinamide (C<sub>6</sub>H<sub>6</sub>N<sub>2</sub>O), nicotinic acid (C<sub>6</sub>H<sub>5</sub>NO<sub>2</sub>), sodium chloride (NaCl), sodium hydroxide (NaOH), hydrochloric acid (HCl), potassium dihydrogen phosphate (KH<sub>2</sub>PO<sub>4</sub>), disodium hydrogen phosphate dihydrate (Na<sub>2</sub>HPO<sub>4</sub>·2H<sub>2</sub>O), sodium azide (NaN<sub>3</sub>), methyl stearate (MEST), trypsin (Bovine), trisodium citrate (Na<sub>3</sub>C<sub>6</sub>H<sub>5</sub>O<sub>7</sub>), citric acid (C<sub>6</sub>H<sub>8</sub>O<sub>7</sub>), Mueller–Hinton (MH) broth, and brain heart infusion (BHI) agar were obtained from Sigma-Aldrich. Methanol (CH<sub>3</sub>OH, HPLC grade), heptane (C<sub>7</sub>H<sub>16</sub>, HPLC grade), formic acid (HCOOH, 99%), and ammonium formate (HCO<sub>2</sub>NH<sub>4</sub>, 99%) were purchased from VWR chemicals (Avantor). Methoxyamine hydrochloride (MOX, CH<sub>3</sub>NO·HCl), N-methyl-N-(trimethylsilyl)trifluoroacetamide (MSTFA), and trimethylchlorosilane (TMCS) were purchased from Thermo Fisher Scientific. Phosphate buffered saline (PBS, pH 7.4) was prepared by mixing 130.9 mM NaCl, 5.1 mM Na<sub>2</sub>HPO<sub>4</sub>·2H<sub>2</sub>O, and 1.5 mM KH<sub>2</sub>PO<sub>4</sub>. Citrate buffer (CBS, pH 5.0) was prepared by mixing 130.9 mM NaCl, 5.81 mM sodium citrate dihydrate, and 4.19 mM citric acid. For both buffers, the pH was adjusted to obtain pH 7.4 (PBS) and pH 5.0 (CBS) by adding aliquots of either 2 M NaOH or 1 M HCl. All aqueous solutions were prepared using ultrapure water with 18.2 MΩ·cm.

### Solubility of niacinamide by UV–Vis spectrophotometry

The solubility of NIA in CBS and PBS was determined at 32 °C by adding an excess amount of NIA to the buffers. NaOH or HCl were added to adjust the pH to 5.0 (CBS) or to 7.4 (PBS). The samples were sealed and incubated at 32 °C for 48 h under constant agitation at 450 rpm. The saturated suspensions were filtered using syringe filters (hydrophilic PVDF, 0.20 μm, 30 mm), discarding the first 0.5 mL of filtrate. The filtrates were then diluted in CBS or PBS as appropriate and analyzed by UV–Visible spectrophotometry. Calibration curves were prepared in the corresponding buffer (i.e., CBS or PBS) using five concentrations between 6 and 40 μg mL<sup>-1</sup>. Absorbance

measurements were performed at 263 nm in a UV-1800 spectrophotometer (Shimadzu) with a quartz cuvette (Hellma Analytics).

### Preparation of full-thickness human skin membranes

Human skin was obtained from three healthy female donors: donor 1 (59 years, breast tissue), donor 2 (38 years, breast tissue), and donor 3 (55 years, abdominal tissue), all of whom underwent plastic surgery and had provided written informed consent. The process was approved by the Swedish Ethics Committee (no. 2018/509-32) and conducted in accordance with the principles of the Declaration of Helsinki. The skin was prepared directly after defrosting and cleaning with PBS buffer (pH 7.4). The skin tissue was trimmed of subcutaneous fat, and full-thickness skin was then punched into circular membranes with a diameter of 16 mm. The membranes were stored at  $-20^{\circ}\text{C}$  on filter paper soaked in PBS and wrapped in aluminum foil until use (maximum three months). Since storage conditions, such as freeze-thaw cycles used here, may influence skin permeability and electrical properties, we treated all human skin with the same storage protocol to allow comparative interpretation of the pH effect<sup>30-34</sup>.

### The EpiDerm human tissue model

The EpiDerm human tissue model (MatTek In Vitro Life Science Laboratories) is a 3D reconstructed epidermal membrane consisting of normal human-derived epidermal keratinocytes cultured on inserts at the air-liquid interface to form a multilayered, differentiated epidermis. The tissue exhibits the major layers of human skin, with organized basal cells, spinous and granular layers, and a cornified SC. The EpiDerm models were obtained in 24-well plates with a membrane diameter of 9 mm. The models were conditioned according to the manufacturer's protocol by incubation in EPI-100-NMM-3 medium on the day they were received. Medium was exchanged every second day with fresh prewarmed medium for 5-6 days prior to usage. For this, a hanging top (HNG-TOP-12) was used. Upon employment, the EpiDerm models were carefully cut out from the insert with a scalpel and mounted on a Franz cell.

### Niacinamide permeation and electrical impedance spectroscopy measurements

Full-thickness human skin membranes were allowed to thaw at room temperature for 30-60 min prior to mounting, while EpiDerm models were taken directly from the culture plates. Next, the membranes were mounted in Franz diffusion cells with diameter of 9 mm (diffusional area of  $0.64\text{ cm}^2$ ) and receptor volume of 6 mL. For experiments using the EpiDerm model, silicone insert rings were used to reduce the Franz cell chamber opening because of the smaller membrane diameter (9 mm). This ensured secure clamping without leakage. The adjustment reduced the effective diffusion area to  $0.23\text{ cm}^2$ , which was used for calculating cumulative permeation. A circulating water bath (HighTech HE-4, Julabo heating circulators) was used to keep the membranes at a constant temperature of  $32^{\circ}\text{C}$  throughout the experiment. Receptor and donor solutions were degassed for 1 h using a sonicator bath (Branson 3210 ultrasonic cleaner) before experiments. The receptor chamber was filled with PBS, while the donor chamber was firstly filled with 1 mL of CBS or PBS for the initial EIS measurements ( $t = 0\text{ h}$ ). Following the initial EIS measurements, the donor solution was replaced with  $800\text{ }\mu\text{L}$  of freshly prepared CBS or PBS buffer containing 5 wt.% NIA. Next, the donor and sampling ports were sealed with parafilm to prevent evaporation. Samples were collected hourly for the first 6 h and at 22 h and 24 h using a Hamilton syringe ( $400\text{ }\mu\text{L}$ ) and analyzed with HPLC. Steady-state fluxes were calculated between 6-24 h due to that a minority of replicates showed non-linear permeation behavior prior to 6 h. After each sampling, an equal volume of fresh PBS was added to the receiver chamber to maintain constant volume. After completion of the experiment, the donor solution was collected for mass balance assessment (see below). Subsequently, the donor solution was replaced with either CBS or PBS for the final EIS measurements ( $t = 24\text{ h}$ ).

A complementary permeation experiment was conducted in which the donor solution pH was alternated between pH 5.0 (CBS) and pH 7.4 (PBS) at 12 h intervals over a total duration of 48 h, using the same skin membrane throughout. Acidic conditions were applied during 0-12 h and 24-36 h, whereas neutral conditions were applied during 12-24 h and 36-48 h. At each pH switch, the donor solution was completely removed and immediately replaced with a freshly prepared buffer at the new target pH; in all cases containing 5 wt.% NIA. Receptor phase aliquots were collected at 8 h, 10 h, and 12 h during the first interval and at the corresponding time points after each subsequent pH change, following the procedure described above. EIS measurements were performed at the start and end of each 12 h interval.

To assess the electrical skin barrier properties, the Franz cells were equipped with four electrodes, connected to a potentiostat from Ivium Technologies. EIS data were collected in the frequency range from 1 Hz to 1 MHz with 5 frequencies per decade. The amplitude of the applied voltage was between 10 and 25 mV to ensure low current densities in the lower frequency range. To interpret EIS data, an electrical equivalent circuit consisting of three elements were employed. These elements reflect the solution resistance ( $R_{\text{sol}}$ ) the membrane resistance ( $R_{\text{mem}}$ ), and a constant phase element (CPE). The  $R_{\text{mem}}$  reflects the resistance to ionic transport across the SC membrane<sup>28,29</sup>. The CPE accounts for the non-ideal capacitive behavior of the skin barrier and was used to calculate the effective capacitance ( $C_{\text{eff}}$ ) of the SC<sup>28,29</sup>. These parameters were derived from the EIS data according to a previously described method<sup>29</sup>. The results are presented as relative changes of membrane resistance ( $\Delta R_{\text{mem}}$ ) and effective capacitance ( $\Delta C_{\text{eff}}$ ), based on the initial ( $i$ ) and final ( $f$ ) impedance data, according to Eqs. 1 and 2.

$$\Delta R_{\text{mem}} (\%) = (R_{\text{mem},f} - R_{\text{mem},i}) / R_{\text{mem},i} \quad (1)$$

$$\Delta C_{\text{eff}} (\%) = (C_{\text{eff},f} - C_{\text{eff},i}) / C_{\text{eff},i} \quad (2)$$

The relationship between the permeability of NIA ( $P$ ) and the electrical resistance of the SC ( $R_{mem}$ ) was evaluated using the logarithmic form shown in Eq. 3, where  $C$  is a proportionality constant<sup>35–37</sup>:

$$\log_{10}P = \log_{10}C - \log_{10}R_{mem} \quad (3)$$

According to Eq. 3, a plot of  $\log_{10}P$  versus  $\log_{10}R_{mem}$  should yield a linear relationship with a slope  $-1$ . To assess whether this relationship applied to the present data set, the permeability coefficients were calculated based on the steady-state fluxes ( $J_{ss}$ ) according to  $P = J_{ss}/\Delta C$ , where  $\Delta C$  corresponds to the concentration gradient across the skin membrane. For these calculations,  $\Delta C$  was assumed to be equal to the donor concentration (i.e.  $5 \times 10^4 \mu\text{g cm}^{-3}$ ). Considering that both  $P$  and  $R_{mem}$  are expected to be continuously influenced by the pH, as well as the fact that the permeability is derived from the time interval between 6 and 24 h, it was decided to use the mean of the initial and final  $R_{mem}$  value in this assessment. Comparable trends were obtained when using either the initial or final  $R_{mem}$  values alone.

### Mass balance analysis

A mass balance evaluation was performed after completion of the permeation experiment to quantify the distribution of NIA between the donor solution, the skin membrane, and the receptor solution. The collected donor solution was weighed to determine the recovered volume (assuming a density of 1.0 g/mL) and analyzed by HPLC–UV. The skin membrane was then removed from the Franz cell, briefly rinsed by immersion in PBS to eliminate residual donor solution, and transferred to a glass vial containing 131 mM NaCl adjusted to pH 12.0 with NaOH (5 mL for human skin; 1 mL for EpiDerm). The sample was sonicated for 1 h to extract NIA, after which the membrane was moved to a new vial containing fresh extraction solution. This extraction cycle was repeated three times to ensure quantitative recovery. The combined extracts were evaporated to dryness under vacuum (miVac concentrator, Genevac), and the residues were reconstituted in 1 mL deionized water for HPLC–UV analysis. The amount of NIA in the receptor chamber was represented by the cumulative permeated mass at 24 h (see above).

### Analysis of microbial conversion of niacinamide into nicotinic acid

To investigate the potential microbial conversion of NIA to nicotinic acid (NA) during the permeation experiments, a subset of experiments were performed with or without 15 mM sodium azide ( $\text{NaN}_3$ ) in the donor solution. After 24 h, skin membranes from both conditions were incubated overnight in MH medium at 32 °C. The next day, aliquots were plated on BHI agar and incubated overnight to evaluate bacterial growth. From the  $\text{NaN}_3$ -free condition, one visible colony-forming unit (CFU) was transferred into 10 mL MH medium containing  $0.7 \text{ mg mL}^{-1}$  NIA. Samples were collected at 2, 4, 6, and 24 h. To confirm bacterial growth, the absorbance was measured at 600 nm with a quartz cuvette. Samples were then centrifuged at 14,000 rpm for 5 min at 4 °C, and the supernatant was transferred to vials and analyzed by HPLC–UV and GC–MS. As a negative control, material from the  $\text{NaN}_3$ -treated plate (which showed no visible growth) was collected by gentle scraping and processed in the same manner.

### Quantification of niacinamide and nicotinic acid by HPLC–UV

Analysis and quantification of NIA and NA were performed using a Vanquish-flex system (Thermo Fisher Scientific) with a VF-P10 binary pump, VH-C10 column compartment, VF-A10 autosampler, and VF-D40 detector. A Luna Omega Polar C18 column ( $100 \times 4.6 \text{ mm}$ ,  $3 \mu\text{m}$  particle size,  $100 \text{ \AA}$  pore size; Phenomenex) was used with a gradient elution profile (see Table S1) with mobile phase A (0.1% formic acid in 10 mM ammonium formate) and mobile phase B (0.1% formic acid in 100% methanol). The injection volume was 10  $\mu\text{L}$ , the flow rate was  $1 \text{ mL min}^{-1}$ , and the column temperature was maintained at 40 °C. The detection wavelength for NIA and NA was 263 nm, and sample concentrations were determined based on a calibration curve consisting of eight concentrations between  $0.586\text{--}1200 \mu\text{g mL}^{-1}$ . Chromeleon 7.3.1 software (Thermo Fisher Scientific) was used for integrating absorbance peaks.

### Gas chromatography–mass spectrometry analysis of niacinamide and nicotinic acid

For gas chromatography–mass spectrometry (GC–MS) analysis, samples were first subjected to protein precipitation using methanol (MeOH). An equal volume of cold MeOH was added to each sample, followed by vortexing and centrifugation at  $14,000 \times g$  for 10 min at 4 °C. The supernatant was carefully transferred to a new vial and dried under vacuum (miVac concentrator, Genevac). Dried samples were stored at 4 °C until derivatization. NIA and NA were derivatized prior to GC–MS analysis to enhance their volatility, chromatographic performance, and thermal stability. For this, 20  $\mu\text{L}$  MOX reagent was added to each vial and shaken for 2 min, followed by a 2 h incubation at room temperature. Next, 20  $\mu\text{L}$  of MSTFA + 1% TMCS were added, followed by 40  $\mu\text{L}$  MEST 5 ppm in heptane. The derivatized samples were then analyzed using GC–MS (GC–MS–TQ8040 from SHIMADZU) with an AOC-20i auto injector. As positive controls, standard solutions of NIA and NA were processed in the same manner to confirm retention times and fragmentation patterns.

### Statistical analysis

Data are presented as mean  $\pm$  SEM (standard error of the mean) unless otherwise stated. Cumulative permeation experiments (human skin and EpiDerm) were analyzed using analysis of covariance (ANCOVA) to assess the effect of pH on cumulative mass permeated over time. Time was treated as a covariate and pH (5.0 vs. 7.4) as a fixed factor. The interaction term (time  $\times$  pH) was included to determine whether permeation rates differed between pH levels across the time course. The flux and impedance data was analyzed with Welch's two-sample

t-tests. A significance level of  $p < 0.05$  was used for all tests. Statistical analyses were performed using R (R Core Team, 2024).

## Results

Skin permeation of NIA was investigated using full-thickness human skin membranes and cultured EpiDerm models, with donor solutions buffered at either pH 5.0 (CBS) or pH 7.4 (PBS), while the receptor solution was buffered at physiological conditions in all cases (i.e., PBS at pH 7.4). Because the pyridine nitrogen of NIA is a weak base ( $pK_a = 3.63$ , estimated using Chemicalize, ChemAxon), its ionization state, and thus its solubility, could in principle vary with pH. This could theoretically affect the chemical potential of NIA associated with a given nominal concentration (here 5 wt.%). To verify that identical applied concentrations correspond to comparable thermodynamic activities under both conditions, we determined the saturation solubility of NIA in CBS and PBS. Triplicate measurements ( $n = 3$ ) showed solubilities of  $46.2 \pm 0.08$  wt.% in CBS (pH 5.0) and  $46.3 \pm 0.32$  wt.% in PBS (pH 7.4), demonstrating no pH dependent variation for the investigated pH values. Given this equivalence, indicating that NIA remains in its neutral form at both pH values, differences in permeation can therefore be attributed to pH dependent effects on the skin barrier, rather than differences in the driving force for NIA diffusion. The high saturation concentration also ensures sink conditions in the receptor phase when 5 wt.% NIA is applied in the donor phase, and the concentration gradient can be assumed equal to the donor concentration.

### Effect of pH on skin permeation of niacinamide

Figure 1 presents the skin permeation data of NIA at the two investigated pH levels.

Starting from the cumulative amount permeated at 24 h, Fig. 1A and C show that pH 7.4 yields higher NIA permeation than pH 5.0 for both full-thickness human skin and the EpiDerm model (ANCOVA, 1–24 h: human skin  $p < 0.001$ ; EpiDerm  $p < 0.05$ ). Because a minority of replicates exhibited non-linear behavior before 6 h, steady-state fluxes were calculated over 6–24 h (Fig. 1B and D). For human skin (Fig. 1B), the average flux was  $56 \pm 14$  and  $22 \pm 9.0 \mu\text{g cm}^{-2} \text{h}^{-1}$  at pH 7.4 and pH 5.0, respectively. For EpiDerm (Fig. 1D), the average flux was  $108 \pm 50$  and  $68 \pm 18 \mu\text{g cm}^{-2} \text{h}^{-1}$  at pH 7.4 and pH 5.0, respectively. These values align well with the slopes from the 1–24 h regressions (Fig. 1A and C), indicating that steady-state conditions are reached rapidly. Collectively, the data show that NIA permeation across both human skin and EpiDerm is enhanced under neutral (pH 7.4) donor conditions relative to acidic (pH 5.0).

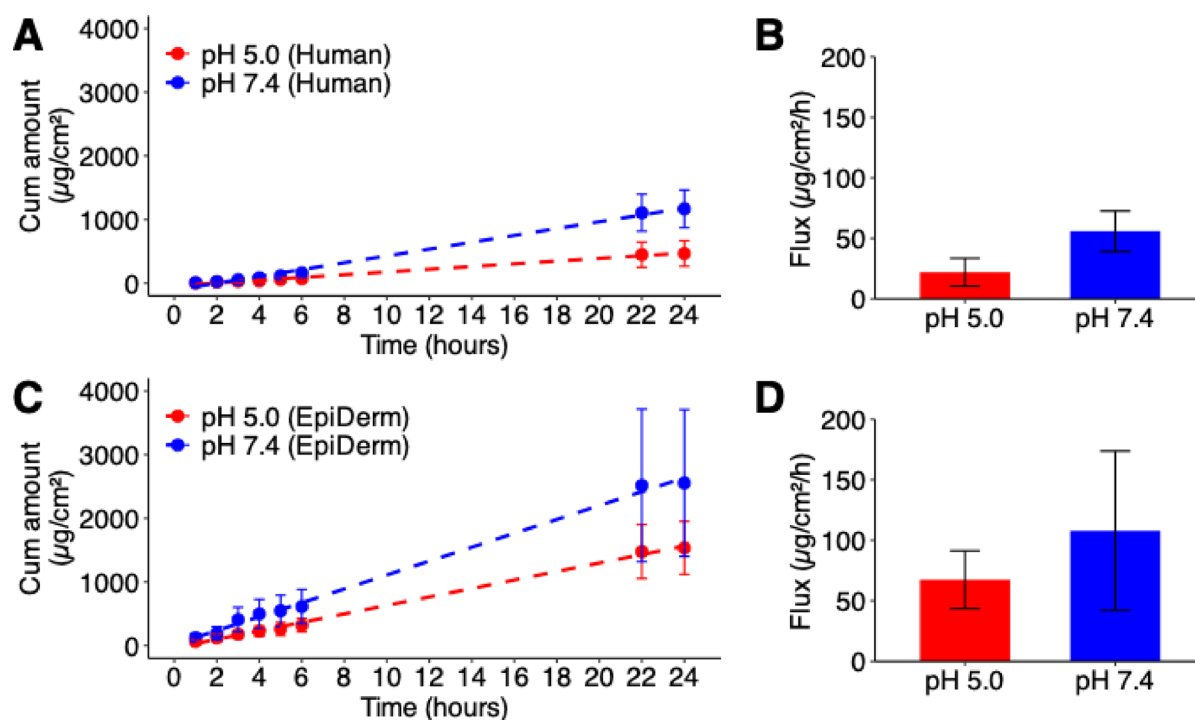


**Fig. 1.** Effect of pH on the skin permeability of NIA. (A) Cumulative permeated mass of NIA for full-thickness human skin membranes (donors 1–3) at pH 5.0 (red) and 7.4 (blue), and (C and D) the corresponding data for the EpiDerm tissue model. Panels (A) and (C) show cumulative permeated mass over time with linear fits applied from 1–24 h. Panels (B) and (D) display steady-state fluxes calculated over 6–24 h. Regression lines in (A) for human skin:  $y = 21x - 39$  ( $R^2 = 0.994$ , pH 5.0),  $y = 54x - 109$  ( $R^2 = 0.994$ , pH 7.4). Regression lines in (C) for EpiDerm:  $y = 67x - 36$  ( $R^2 = 0.997$ , pH 5.0),  $y = 109x + 17$  ( $R^2 = 0.996$ , pH 7.4). Replicates: human skin,  $n = 11$  (pH 5.0) and  $n = 19$  (pH 7.4); EpiDerm,  $n = 8$  (pH 5.0) and  $n = 6$  (pH 7.4).

	Human		EpiDerm	
	pH 5.0 ( <i>n</i> =11)	pH 7.4 ( <i>n</i> =13)	pH 5.0 ( <i>n</i> =8)	pH 7.4 ( <i>n</i> =6)
Permeation % (mg cm <sup>-2</sup> )	0.65 ± 0.27 (0.46 ± 0.19)	2.05 ± 0.51 (1.37 ± 0.36)	1.09 ± 0.26 (1.24 ± 0.39)	1.49 ± 0.58 (2.52 ± 1.00)
Extraction % (mg cm <sup>-2</sup> )	0.16 ± 0.09 (0.11 ± 0.06)	0.29 ± 0.10 (0.20 ± 0.06)	0.22 ± 0.04 (0.31 ± 0.06)	0.13 ± 0.02 (0.19 ± 0.03)
Donor %	95 ± 4	97 ± 2	100 ± 4	108 ± 2
Mass balance %	96 ± 4	99 ± 2	101 ± 4	110 ± 2

**Table 1.** Mass balance (%) of NIA from the permeation experiments with split-thickness human skin (donors 1–3) and the EpiDerm tissue model. The table summarizes the distribution of NIA into four components: permeated amount, extracted amount from the membrane, remaining amount in the donor, and the resulting total mass balance (reported as % of the applied dose). For permeation and extraction, values are reported both as percentages and, in parentheses, as mass per unit area (mg cm<sup>-2</sup>). Replicate numbers (*n*) are indicated for each condition.

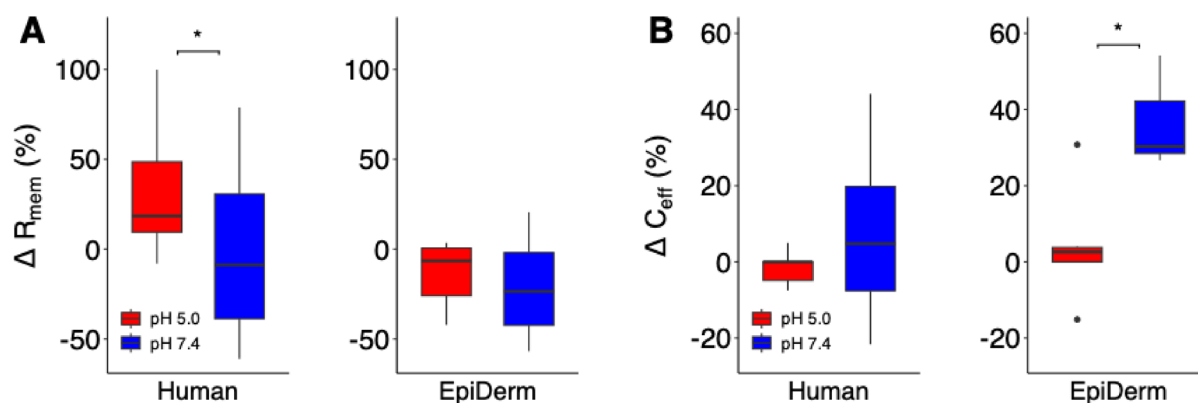


**Fig. 2.** Effect of pH on the electrical skin membrane properties. (A) Relative changes in membrane resistance ( $\Delta R_{\text{mem}}$ ) and (B) effective capacitance ( $\Delta C_{\text{eff}}$ ) for full-thickness human skin membranes (donors 1–3) and the EpiDerm tissue models following 24 h exposure of pH 7.4 (PBS) or pH 5.0 (CBS) conditions. Boxes represent the interquartile range with medians shown as horizontal lines. Number of replicates: human skin, *n*=8 (pH 5.0) and *n*=17 (pH 7.4); EpiDerm, *n*=7 (pH 5.0) and *n*=4 (pH 7.4).

Table 1 summarizes the mass balance analysis of NIA following the permeation experiments, accounting for NIA that permeated into the receptor phase, was extracted from the skin membrane, or remained in the donor solution. The total recovery was approximately 100% of the applied dose across all experimental conditions, confirming that the mass balance was within acceptable limits and supporting the reliability of the permeation protocol. At both pH 5.0 and pH 7.4, the majority of NIA remained in the donor compartment, consistent with infinite dose conditions.

In full-thickness human skin, higher permeability at pH 7.4 was accompanied by greater NIA retention in the membrane, whereas lower permeability at pH 5.0 was associated with lower extracted amounts. This relationship was not observed in the EpiDerm model, which showed lower extracted NIA at pH 7.4 despite higher permeability. Comparing models, EpiDerm displayed higher percentages of permeated and extracted NIA than full-thickness human skin at pH 5.0, but lower percentages at pH 7.4. However, when considering absolute (area-normalized) amounts, permeated and extracted NIA were generally higher in EpiDerm than in human skin, except for the extracted amount at pH 7.4. This pattern indicates that the dermis of full-thickness human skin does not act as a significant sink for NIA under these conditions and that the extracted amounts arise primarily from epidermal partitioning.

### Effect of pH on electrical properties of the skin barrier

In parallel with the permeation studies, EIS measurements were performed to characterize the effect of pH on the relative changes of skin membrane resistance (i.e.,  $\Delta R_{\text{mem}}$ ) and effective capacitance ( $\Delta C_{\text{eff}}$ ) following 24 h exposure to either pH 5.0 (CBS) or pH 7.4 (PBS). The results from this analysis are presented in Fig. 2.

Focusing on the effect of pH on the electrical membrane resistance, Fig. 2A shows that acidic pH results in an increase of  $\Delta R_{\text{mem}}$  for human skin membranes, whereas it causes a slight decrease in the EpiDerm model. Neutral pH, however, produces more pronounced decreases in  $\Delta R_{\text{mem}}$  for both skin models. For human skin,  $\Delta R_{\text{mem}}$  was significantly higher at pH 5.0 than at pH 7.4 ( $p < 0.05$ ). No statistically significant difference was observed for the EpiDerm tissue model ( $p = 0.17$ ).

The effect of pH on the effective capacitance is presented in Fig. 2B.  $\Delta C_{\text{eff}}$  remained relatively unchanged at pH 5.0 for both human skin and the EpiDerm model. In contrast, exposure to pH 7.4 resulted in an increase of  $\Delta C_{\text{eff}}$  for both skin models, although the variability was substantial. When comparing the two pH conditions, a significant increase in  $C_{\text{eff}}$  was observed only in the EpiDerm model ( $p < 0.05$ ), whereas no statistically significant change was detected in human skin ( $p = 0.12$ ).

### Switching between acidic and neutral pH conditions

Although the results in Figs. 1 and 2 reveal clear pH effects on NIA permeability and electrical properties of the SC, the results suffer from a substantial biological variability of the skin membranes. To minimize the impact of this natural variability and facilitate the interpretation of the pH effect, we designed a complementary set of experiments in which consecutive data are generated from human skin membranes with the pH as the varying parameter. In this so-called switch experiment, the pH of the donor phase was repeatedly alternated between acidic and neutral pH conditions for 12 h periods, with a total experimental time of 48 h (i.e., two 12 h periods per pH level). The results from these experiments are presented in Fig. 3.

Figure 3A shows the cumulative permeation of NIA across full-thickness human skin, and Fig. 3B presents the corresponding interval-based fluxes. Although the absolute fluxes observed in Fig. 3B are lower than those in Fig. 1B, the relative trend is preserved, showing that the permeability remained lower at pH 5.0 than at pH 7.4 across all switch intervals. This confirms the overall trend that NIA permeability is lower under acidic donor conditions compared to neutral conditions. It is noteworthy that all membranes used in this experiment were obtained from donor 3, a donor characterized by consistently lower permeability compared to donors 1 and 2 under both pH conditions. Such variation lies within the expected range for ex vivo human skin and may arise from donor-specific characteristics, differences introduced during membrane preparation, or other inherent sources of experimental variability.

The EIS measurements (Fig. 3C and D) likewise mirror the patterns observed in Fig. 2A and B. Exposure to pH 5.0 increased  $\Delta R_{\text{mem}}$ , whereas pH 7.4 reduced  $\Delta R_{\text{mem}}$  (Fig. 3C). For  $\Delta C_{\text{eff}}$  values remained stable at pH 5.0, while pH 7.4 generally induced an increase, albeit with considerable variability (Fig. 3D). Together, these findings demonstrate that both permeability and electrical parameters exhibit reproducible and reversible pH dependent behavior.

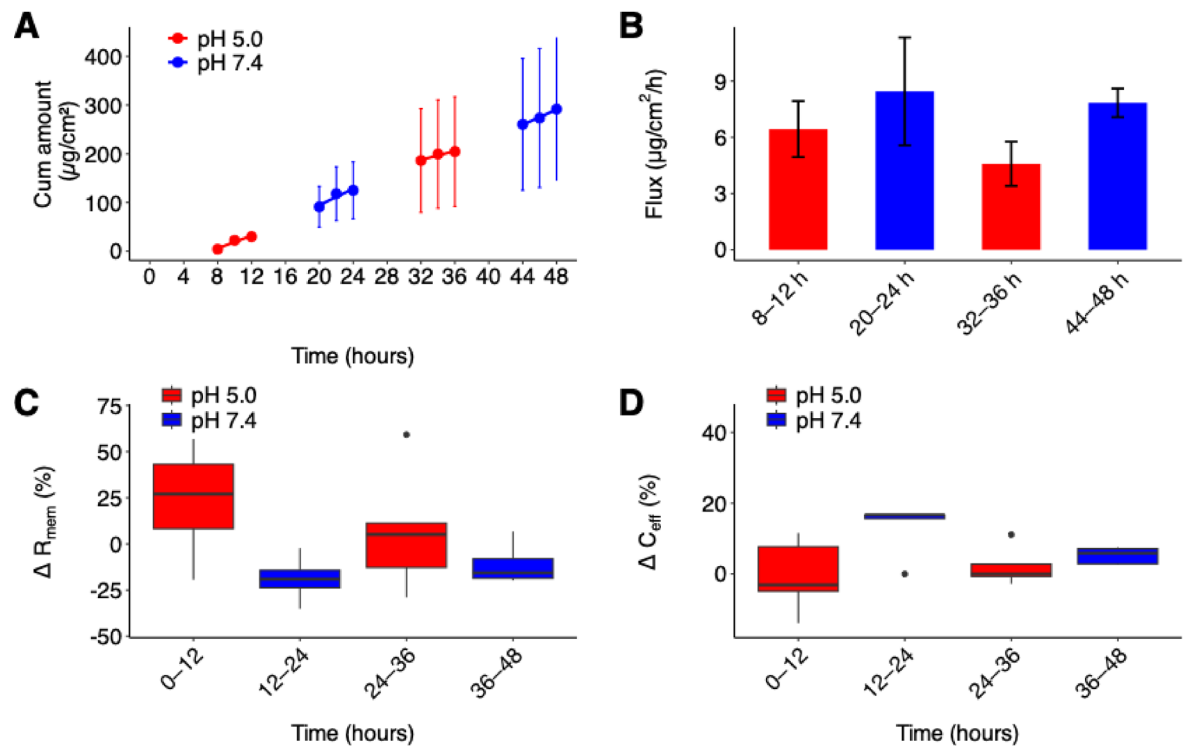


**Fig. 3.** Effect of consecutive pH switching on NIA permeability and electrical properties of human skin. (A) Cumulative permeated amounts of NIA at pH 5.0 (red) and pH 7.4 (blue). (B) Corresponding fluxes calculated for each 12-h interval (8–12, 20–24, 32–36, and 44–48 h). (C) Relative changes in membrane resistance ( $\Delta R_{\text{mem}}$ ) and (D) effective capacitance ( $\Delta C_{\text{eff}}$ ) for the corresponding consecutive time intervals. Boxes in (C) and (D) indicate the interquartile range, with medians shown as horizontal lines. All measurements were performed using full-thickness human skin membranes from donor 3 ( $n = 5$ ), which were used throughout the entire pH switch experiment.

### Microbial conversion of niacinamide into nicotinic acid under long-term experimental conditions

An interesting observation from the prolonged permeability experiments with consecutive switching between pH conditions is that the transport rate of NIA tends to decrease over time when comparing consecutive intervals (see Fig. 3B). For example, at pH 5.0 in Fig. 3B, the average flux between 32–36 h is lower than that between 8–12 h. Normally, prolonged exposure to aqueous donor solutions results in increased skin permeability over time<sup>38</sup>, making this an unexpected finding. These experiments were performed without any bacteriostatic or enzyme-inhibiting compounds, suggesting that microbial growth or enzymatic activity could be involved<sup>39</sup>. To investigate this, the HPLC–UV chromatograms of the collected receptor samples were further analyzed, revealing the emergence of a new peak around 24 h, which increased in intensity over time (Fig. 4A). This suggests that NIA undergoes conversion to another compound, leading us to hypothesize microbial transformation of NIA into NA<sup>40</sup>. To test this hypothesis, we performed a second set of diffusion experiments with sodium azide (15 mM  $\text{NaN}_3$ ) added to both donor and receptor solutions. In the presence of  $\text{NaN}_3$ , the suspected NA peak did not appear, whereas it continued to develop without  $\text{NaN}_3$ , indicating microbial conversion of NIA to NA. It is, however, important to point out that the impact of this conversion of NIA to NA on the overall permeated amount of NIA after 24 h is negligible (less than 0.05% of the applied NIA and 1–2% of the permeated NIA amount). To confirm microbial contamination, skin membranes were incubated in MH broth and plated on agar. Bacterial growth occurred only in samples without  $\text{NaN}_3$ . A colony was isolated and cultured in MH broth containing NIA ( $0.7 \text{ mg mL}^{-1}$ ). Periodic HPLC–UV analysis of this culture revealed a decline in NIA concentration, accompanied by the emergence of a peak corresponding to NA (Fig. 4B). Finally, GC–MS was employed to establish the presence of NA in the experiment without  $\text{NaN}_3$ , with a peak matching its retention time and MS spectrum after 24 h (Fig. S1).

### Correlation between niacinamide permeation and skin membrane resistance

Because the diffusivity of small polar molecules and ions is inversely related to solution viscosity, the porous-pathway model predicts that their permeability should scale proportionally with electrical conductance and inversely with membrane resistance. Consistent with this, previous studies have reported good correlations between the permeability coefficients of small hydrophilic substances, such as mannitol, urea, and sucrose, as well as passive diffusion of  $\text{Na}^+$  ions, and the electrical resistance of the SC<sup>35–37,41,42</sup>. Using the present experimental design, which provides paired measurements of NIA permeability and SC electrical resistance, we evaluated whether a similar relationship exists for NIA. According to Eq. 3, an inverse log–log relationship with a slope of  $-1$  is expected if transport occurs through aqueous pathways consistent with porous-pathway behavior<sup>35–37</sup>. As shown in Fig. 5, the data exhibited a clear inverse relationship between the permeability coefficient for NIA and  $R_{mem}$ , broadly consistent with this theoretical expectation.

The data in Fig. 5 span a wide range of  $P$  and  $R_{mem}$  values, reflecting large biological variability in barrier properties of individual membranes. However, pH does not appear to separate the data into distinct groups, indicating that pH modulates the skin permeability of NIA and charge carrier in the same manner. Further, the data from human skin and the EpiDerm model follow similar linear trends. To determine whether permeability and electrical resistance are quantitatively related, we applied ANCOVA. Across all conditions, we found a consistent negative correlation when combining all data (Fig. 5A), with similar patterns observed separately for

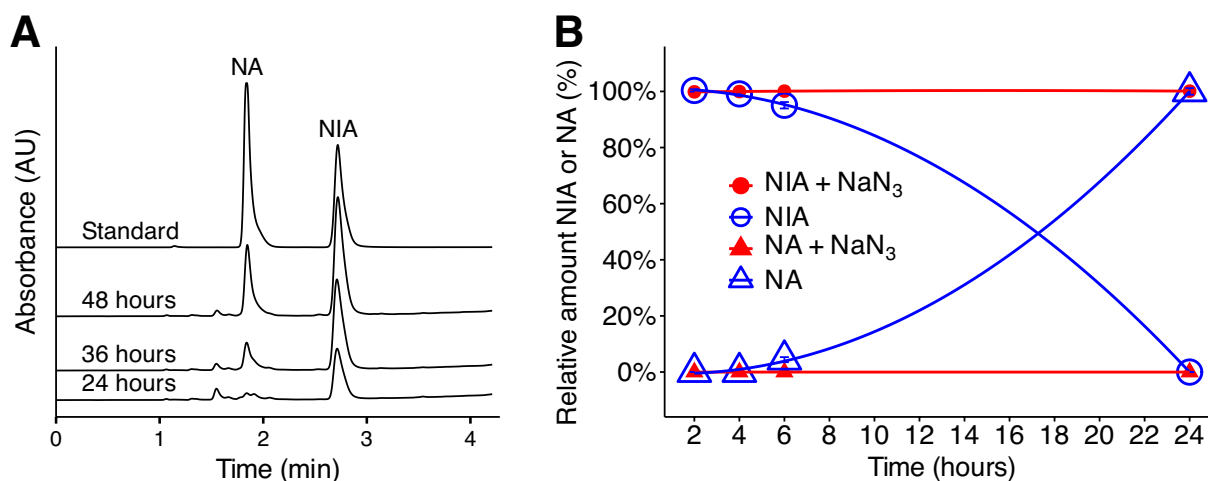


**Fig. 4.** Microbial conversion of NIA to NA during prolonged permeation experiments without  $\text{NaN}_3$ . (A) HPLC–UV chromatograms, corresponding to standard solution of NIA and NA (both at  $1.2 \text{ mg mL}^{-1}$ ) with retention times of 2.7 and 1.8 min, respectively (top). Chromatograms below, from bottom to top, correspond to samples collected from the receptor phase at 24, 36, and 48 h, respectively. (B) Confirmation of microbial conversion of NIA to NA as a function of time in bacterial cultures collected from skin membranes after a 24 h permeation experiment with (red) and without  $\text{NaN}_3$  (blue) in MH broth containing an initial NIA concentration of  $0.7 \text{ mg mL}^{-1}$ . Solid lines in (B) are shown for visual guidance only.

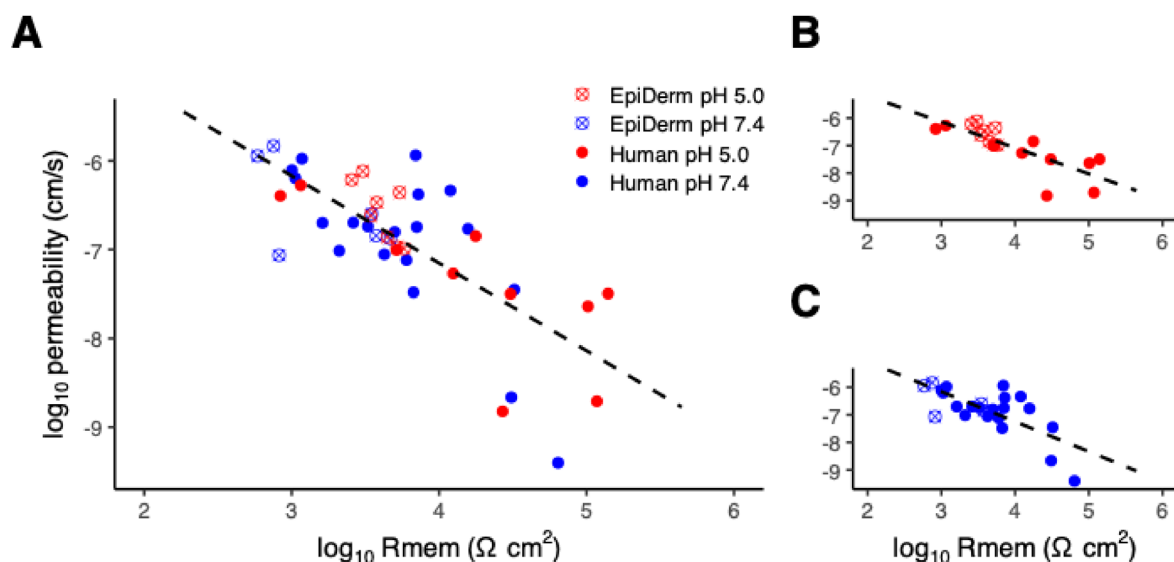


**Fig. 5.** Correlation between NIA permeation ( $P$ ) and electrical skin membrane resistance ( $R_{\text{mem}}$ ) in logarithmic coordinates (in accordance with Eq. 3), including both human skin and EpiDerm model. **(A)** All data ( $n = 43$ , where each point representing a pair of  $P$  and  $R_{\text{mem}}$  values for a single skin membrane (regression line:  $\log P = -0.98 \pm 0.14 \log R_{\text{mem}} - 3.2$ ,  $R^2 = 0.56$ ). **(B)** Subset ( $n = 18$ ) for pH 5.0 (regression line:  $\log P = -0.94 \pm 0.18 \log R_{\text{mem}} - 3.3$ ,  $R^2 = 0.63$ ). **(C)** Subset ( $n = 25$ ) for pH 7.4 (regression line:  $\log P = -1.09 \pm 0.22 \log R_{\text{mem}} - 2.9$ ,  $R^2 = 0.52$ ).

	Permeability coefficient ( $\text{cm s}^{-1}$ )	
	pH 5.0	pH 7.4
Experiment (Human Skin)	$13 \pm 6 \times 10^{-8}$	$31 \pm 8 \times 10^{-8}$
Experiment (EpiDerm)	$34 \pm 9 \times 10^{-8}$	$54 \pm 25 \times 10^{-8}$
Theoretical prediction A (Eq. S1)	$4.6 \times 10^{-8}$	$4.8 \times 10^{-8}$
Theoretical prediction B (Eqs. S2-S5)	$8.5 \times 10^{-8}$	$8.7 \times 10^{-8}$

**Table 2.** Summary of experimental and predicted skin permeability coefficients of NIA.

human skin and EpiDerm at both pH 5.0 (Fig. 5B) and pH 7.4 (Fig. 5C). There were no statistically significant differences among any experimental groups. Consequently, these results demonstrate that the correlation between NIA permeability and electrical resistance is consistent across skin membrane type and pH condition and supports the idea that passive diffusion of NIA and charge carriers are governed by common transport hindrance and structural constraints within the SC barrier. Strikingly, this finding is valid for both full-thickness human skin and the EpiDerm model.

### Comparison of experimental and theoretical skin permeability coefficient of NIA

To compare the experimentally determined skin permeability coefficients of NIA at acidic and neutral conditions with those theoretically predicted, we employed two common models to predict the theoretical skin permeability coefficient of NIA (see supporting text S1 for details)<sup>43</sup>. The experimental and predicted values are compiled in Table 2.

In brief, the first prediction (A in Table 2) is based on the Potts and Guy equation, which is an empirical quantitative structure–permeability (QSPR) model widely applied in transdermal drug delivery for estimating the permeability of small molecules<sup>44</sup>. The model predicts the skin permeability as a function of lipophilicity and molecular size and assumes solute transport exclusively through the lipid domains of the SC. As shown in Table 2, this model underpredicts the observed transdermal permeability of NIA. This suggests that additional pathways, such as aqueous channels or appendageal routes (i.e., hair follicles and sweat ducts), may contribute to NIA permeation. To accommodate these transport routes, the second prediction (B in Table 2) is based on the four permeation pathways model, accounting for diffusion via free-volume and lateral diffusion in the SC lipid matrix, diffusion through aqueous pores created by imperfections in the lipid matrix, and diffusion through shunt pathways<sup>45</sup>. As shown in Table 2, this model predicts approximately twice the skin permeability of NIA compared to the Potts and Guy model and is in better agreement with the experimentally measured value at pH 5.0 for human skin membranes. However, the experimentally measured value at neutral pH for human skin, as well as at both pH conditions for EpiDerm model, are consistently higher than the theoretical values. These

discrepancies are not surprising, as these theoretical models do not explicitly account for perturbations of the SC barrier, such as hydration- and pH induced alterations in the phase behavior of the lipid matrix and corneocytes.

## Discussion

### The pH gradient regulates skin permeation of niacinamide

NIA permeation was consistently higher at neutral pH across both human skin and EpiDerm model (Fig. 1), indicating that pH strongly influences the SC barrier properties. Although absolute fluxes differed between the two models, the relative pH effect was similar, highlighting that the EpiDerm model recapitulates the qualitative functional response of native human skin. The pH switch experiment (Fig. 3) further demonstrated that donor pH can reversibly modulate NIA permeability. Consistent with these findings, passive permeation of hydrophilic compounds such as glucose, tryptophan, and kynurenine across pig epidermis has been shown to be elevated at neutral pH than at pH 5.0<sup>39,46</sup>. In contrast, a previous study on skin permeation of the hydrophobic substances hydrocortisone ( $\log P = 1.61$ ) and testosterone ( $\log P = 3.32$ ) found no significant change in flux for either drug over an extremely wide pH range of 1–11<sup>47</sup>. Together, these data suggest that hydrophilic permeants utilize transport pathways that are more sensitive to pH induced structural changes than those used by hydrophobic permeants.

Before interpreting these effects mechanistically, it is important to note that in our experiments the donor solutions had essentially identical water activity (i.e.,  $a_w \approx 0.99$  for both CBS and PBS)<sup>38</sup>. As a result, the water activity is uniform throughout the system at equilibrium, even though local water content differs among SC compartments. At these conditions, the SC lipid headgroup regions take up only limited water, on the order of two molecules per lipid, likely arising from strong headgroup hydrogen bonding and interdigitation of very-long chain lipids across apposed leaflets<sup>29,48–52</sup>. In contrast, corneocytes swell substantially upon hydration<sup>53,54</sup>. Hydration can mobilize both SC lipids and keratin filaments, thereby increasing permeant partitioning and diffusion in the SC<sup>29,38,55–57</sup>. Since the water activity is matched for both donor pH values, these hydration effects are expected to be equivalent in both cases and therefore cannot account for the observed pH dependent differences in NIA permeability.

At a donor pH of 7.4, the proton activity (and therefore the pH) is uniform across the skin membrane at equilibrium. In contrast, even when the pH boundary conditions are fixed, local proton concentrations within the SC can still vary because of interactions with charged lipid and protein molecular segments, as well as the exclusion of protons from hydrophobic domains. For donor pH 5.0, a pH gradient is established across the membrane (from  $\sim 5.0$  at the SC surface toward  $\sim 7.4$  in the receptor), such that the outermost SC reflects the donor pH while deeper regions rise toward neutrality. Thus, under these controlled hydration conditions, NIA permeation is governed by pH effects that may influence the available transport pathways across the SC, rather than by hydration effects. Although NIA may permeate both corneocytes and the surrounding lipid matrix, only the latter provides a continuous pathway across the SC<sup>1–4,43,45</sup>, while shunt routes such as hair follicles and sweat glands contribute only marginally under our conditions (see Table S3 and discussion below)<sup>43,45</sup>. Consequently, NIA must traverse lipid domains, whose structure and phase behavior govern partitioning and diffusion<sup>1–4,43,45</sup>. The native SC lipid matrix, composed of very long, mostly saturated free fatty acids and ceramides, together with cholesterol, is highly ordered and solid-like.<sup>3</sup> This organization imposes a substantial diffusional resistance and limited partitioning of hydrophilic molecules<sup>1,2,4,43–45,58–60</sup>. Even so, small fractions of fluid lipid domains and structural defects at domain boundaries can disproportionately enhance permeability by locally increasing partitioning and reducing diffusional resistance<sup>4,50,57,61,62</sup>.

Here, it should be noted that 3D reconstructed skin models often exhibit altered lipid profiles compared to native SC, including reduced free fatty acid levels, shorter ceramide and fatty acid chain lengths, and elevated proportions of unsaturated ceramides<sup>63</sup>. These changes modify the phase behavior and reduce the ordering of the lipid matrix, which typically results in higher permeability than native human skin,<sup>63</sup> consistent with our observations in the present study.

Against this background, a plausible mechanistic contributor to the observed pH effect is the protonation state of free fatty acids, the only titratable lipid class in the SC lipid matrix. The intrinsic pKa of long-chain free fatty acids (e.g., palmitic, stearic) in molecular solution is around 4.8–5.0<sup>64</sup>, whereas apparent pKa values increase substantially when fatty acids are incorporated at lamellar interfaces<sup>65–67</sup>. Studies on SC lipid mixtures report apparent pKa around 6.2–7.3<sup>68</sup>. Increasing the pH to this pKa window increases fatty acid ionization and produces a small but detectable reduction in chain order<sup>68</sup>. In line with this, pH dependent changes in the SC lipid lamellar organization are observed with mixtures containing ceramides, cholesterol, and fatty acids, whereas no such effect is observed when fatty acids are excluded<sup>27</sup>. Accordingly, under our experimental conditions, fatty acids are expected to be predominantly protonated at pH 5.0 and partially deprotonated at pH 7.4. This partial deprotonation can alter the interfacial packing and create defective microdomains in the SC lipid matrix, thereby providing a mechanistic explanation for the enhanced NIA permeability at neutral pH.

The pronounced swelling of corneocytes upon hydration indicates that the cornified envelope and its associated lipid monolayer permit permeation of water molecules, suggesting that NIA may likewise penetrate and accumulate within corneocytes. Consistent with this, NIA has been shown to increase keratin monomer spacing, implying partitioning into the corneocyte interior<sup>10</sup>. Reports of preferential accumulation of mercury ions in corneocytes, likely via partially degraded corneodesmosomes, further demonstrate that small polar species can access corneocyte interiors<sup>60</sup>. Together, these observations suggest that the corneocytes may act as a reservoir for hydrophilic substances, such as NIA. However, because corneocytes are discrete domains embedded within the continuous lipid matrix, altered diffusion within corneocytes alone is unlikely to explain the observed pH dependent permeability effects, indicating that transcellular transport contributes only marginally under the conditions studied.

Given the higher permeation at neutral pH, greater partitioning of NIA within the skin membrane was anticipated. This was confirmed for human skin membranes (Table 1). The enhanced partitioning of NIA at neutral pH is consistent with our previous findings, where SC samples equilibrated at pH 7.4 with 5 wt.% NIA exhibited strong diffraction peaks from crystalline NIA after drying, whereas samples equilibrated at pH 5.0 did not<sup>10</sup>. These observations indicate that neutral pH promotes NIA uptake into the SC, leading to oversaturation and crystalline depot formation upon drying. Collectively, these results suggest that NIA penetrates and partitions more efficiently at neutral pH than at acidic pH in human skin. However, this outcome was not observed for EpiDerm model (Table 1), despite the fact that neutral pH resulted in higher NIA permeability. A limitation is the small number of replicates ( $n = 6-8$ ) in the case of EpiDerm, and additional experiments are needed to confirm the pH effect on NIA partitioning inside this tissue model.

### The effect of pH on the electrical properties of the skin barrier

EIS has previously been employed to investigate the effect of various external parameters on the SC electrical properties, such as hydration<sup>29,69,70</sup>, skin storage conditions<sup>30</sup>, mechanical damage<sup>71</sup>, and UV radiation in combination with oxidative stress<sup>72,73</sup>. Of particular relevance is the combination of EIS and permeation data, where the SC electrical resistance is expected to correlate with permeation of small hydrophilic molecules<sup>30,35,36,41,42</sup>, while the effective skin capacitance has been shown to correlate better with transport of hydrophobic permeants<sup>30</sup>.

The skin resistance ( $R_{\text{mem}}$ ) reflects the diffusional resistance to ion transport within the membrane at frequencies approaching direct current. Our results show that pH has a pronounced effect on  $R_{\text{mem}}$  (Fig. 2A), with values approximately 2–4 times lower under neutral conditions. Switch experiments confirm that this pH effect is reversible; however,  $R_{\text{mem}}$  gradually decreases over time at neutral conditions (Fig. 3C). To interpret these changes, it is important to consider ion distribution within the SC and its response to pH alterations. Previous studies suggest that ions are primarily transported and distributed in the lipid matrix<sup>29,60,74</sup>. Thus, the reduction in  $R_{\text{mem}}$  indicates alterations in the lipid domains of the SC, such as the aforementioned partial deprotonation of free fatty acids at neutral conditions. This pH effect could promote formation of defective microdomains that form conductive regions, effectively contributing to the observed decrease in  $R_{\text{mem}}$ .

Prolonged hydration of the SC, such as in the present experiments, often leads to the appearance of water inclusions (i.e., water pools of varying size) within the tissue and may indicate partial tissue disintegration. This phenomenon has been observed in several studies employing different microscopy techniques<sup>53,75–77</sup>. In principle, such tissue disintegration could result in free diffusion of hydrophilic charge carriers, effectively giving rise to resistance values approaching  $R_{\text{sol}}$ . However, this is not the case in our experiments, where  $R_{\text{mem}}$  values tend to increase at pH 5.0 and decrease at pH 7.4, even though both donor conditions imposed the same hydration effect (i.e.,  $a_w \approx 0.99$ ). Further, the reduction in  $R_{\text{mem}}$  at neutral pH, and the associated increase in NIA permeation, are not changes of orders of magnitude, as would be expected in the case of complete tissue disintegration. This indicates that any aqueous inclusions formed between corneocytes during prolonged hydration contribute little to the overall transport of hydrophilic charge carriers or polar permeants, while the principal barrier element, represented by the continuous lipid matrix, remains relatively intact.

The effective capacitance ( $C_{\text{eff}}$ ) of the skin membrane is related to the dielectric properties of the SC, which includes both the low conductivity lipid matrix and the presence of charged lipid and protein species that contribute to double-layer capacitance<sup>29,78</sup>. The results show a clear and reversible effect, with enhanced  $C_{\text{eff}}$  values at neutral conditions and reduced values at acidic conditions (Figs. 2B and 3D). As discussed above, we propose that neutral pH promotes partial deprotonation of free fatty acids, thereby increasing the charge density within the headgroup regions of the SC lipid lamellae matrix. A higher charge density is expected to raise  $C_{\text{eff}}$  by providing additional sites for double-layer charging. In addition, protein components of the SC may also contribute to capacitive currents, where charged amino acid residues in mobile terminal domains of keratin filaments are expected to be accessible for double-layer charging<sup>29,78</sup>. In SC, keratin K1 and K10 dominates, with isoelectric points around 5.3 and 4.9, respectively (UniProt accession: P04264 and P13645). However, for double layer charging, it is the total number of charged sites, not just the net charge, that determines the overall contribution. Sequence-based estimates indicate that the total number of charges only changes slightly between pH 5.0 and 7.4, with the net charge becoming more negative at neutral pH. Thus, the observed increase in  $C_{\text{eff}}$  at neutral pH likely stems primarily from partial deprotonation of free fatty acids, which enhances double-layer charging and thereby increases  $C_{\text{eff}}$  under neutral conditions.

### Influence of acidic and neutral pH on niacinamide and ion skin permeation

Previous studies have explored the aqueous pore pathway hypothesis to explain transport of hydrophilic solutes across the SC. The pore pathway has been proposed to involve structural imperfections in the SC lipid matrix, such as grain boundary separations or lattice vacancies forming transient hydrophilic channels<sup>37,45</sup>. Peck et al. estimated the average aqueous pore radius in untreated and ethanol-treated human epidermal membrane for four small hydrophilic permeants (urea, mannitol, sucrose, and raffinose) using dual-radiolabeled diffusion experiments<sup>79</sup>. By assuming that paired permeants traverse the same aqueous channels, porosity ( $\epsilon$ ) and tortuosity ( $\tau$ ) were eliminated as variables, leaving pore radius as the sole unknown<sup>79</sup>. Building on this, Tang et al. combined the aqueous pore pathway hypothesis with electrochemical principles to predict mannitol and sucrose permeability from skin electrical resistance measurements, enabling determination of pore radius in untreated and ultrasound-treated pig skin and human skin membranes<sup>35</sup>. Tezel et al. refined the model to account for deviations observed with larger hydrophilic permeants, allowing prediction of their permeability in untreated and ultrasound-treated pig skin membranes using electrical resistance data<sup>37</sup>. Kushner et al. further broadened the framework by examining transport of multiple radiolabeled hydrophilic solutes (urea, mannitol, raffinose, and inulin) to independently determine porosity, tortuosity, and hindrance factor for full-thickness human

skin membranes<sup>80</sup>. Electrical resistance measurements were collected in parallel as an independent indicator of barrier perturbation by sonophoresis and SDS treatment<sup>80</sup>. In particular, their analysis showed that decreases in skin resistance were dominated by large increases in porosity and modest decreases in tortuosity, while pore radius remained essentially unchanged<sup>80</sup>. This indicates that skin resistance is governed predominantly by the porosity-to-tortuosity ratio rather than pore size.

Coherent with these findings, NIA permeability was inversely correlated with skin resistance, with slopes near  $-1$ , consistent with Eq. 3 (Fig. 5)<sup>35–37</sup>. Notably, in our data the intercepts for both pH 5.0 and pH 7.4, across human skin and EpiDerm model, align on the same regression line. In contrast, changes in the pore radius are expected to shift the intercept values, whereas variations in porosity, tortuosity, and membrane thickness do not<sup>35,37</sup>. Thus, the results indicate that pH does not significantly affect the effective pore radius, while variations in porosity and tortuosity seem more likely to explain the pH effect (assuming that the SC thickness remains unchanged)<sup>35,37</sup>. Porosity refers to the proportion of membrane volume taken up by pores, whereas tortuosity reflects the deviation of pore pathways from a straight route through the membrane. The porosity-to-tortuosity ratio ( $\epsilon/\tau$ ) indicates pore network efficiency: higher values mean more or straighter pores for faster transport, while lower values mean fewer or more convoluted pores that slow diffusion. From Table 2, the permeability coefficients are approximately twofold higher at pH 7.4, implying that  $\epsilon/\tau$  is roughly twice as high under neutral conditions. Furthermore, because skin electrical resistance is inversely proportional to  $\epsilon/\tau$ <sup>35,37</sup>, the fourfold higher resistance observed in human skin and twofold higher resistance in the EpiDerm model at pH 5.0 (Fig. 5) further supports this interpretation. These findings also indicate that pH dependent changes in  $\epsilon/\tau$  disproportionately affect ionic transport relative to NIA diffusion. Taken together, this suggests that pH modulates the number of available pores and/or the connectivity of the porous pathways rather than enlarging individual pores. As discussed above, a plausible mechanism is that at neutral pH, partial deprotonation of free fatty acids induces electrostatic repulsion between lipid headgroups, effectively promoting localized defective microdomains that enhance  $\epsilon/\tau$  at neutral conditions.

To further evaluate our data according to the aqueous pore pathway framework, we aimed at estimating the pore size by extrapolating each data point in Fig. 5 to the y-axis, assuming a theoretical slope of  $-1$  (see supporting text S2)<sup>35,37</sup>. However, the calculated intercepts were much higher than expected, indicating that NIA permeates more readily than electrolytes. Consequently, the extrapolated pore size becomes unrealistically large, diverging toward infinity, which reflects a breakdown of the steric exclusion assumption. This suggests that NIA permeation cannot be explained solely by the pore pathway and likely involves additional diffusion routes. Our moderate correlation coefficients ( $R^2 = 0.52–0.63$ , see Fig. 5) support this interpretation, as stronger correlations have been reported for highly hydrophilic molecules ( $R^2 = 0.75–0.96$ )<sup>35–37</sup>, whereas lipophilic compounds such as corticosterone ( $\log P = 2.1$ ) show minimal correlation ( $R^2 = 0.30$ )<sup>36</sup>. Thus, the porous pathway primarily applies to highly hydrophilic permeants, while the intermediate polarity of NIA implies multiple diffusional routes, with only partial pore pathway contribution<sup>45</sup>. To quantify these contributions, we applied the four permeation pathways model, which considers free-volume and lateral diffusion in the lipid matrix, shunt pathway, and the aqueous pore pathway (see supportive text S2 and Table S3)<sup>45</sup>. Approximately 46–48% of NIA permeation was attributed to pores, while 51–52% occurred via lipoidal free-volume diffusion; other routes were negligible. Adjusting experimental permeability for this partial pore contribution, the experimental permeability coefficients were proportionally adjusted to obtain revised intercept values that were employed in Eq. S10. Using this approach, the estimated pore radius was 10 Å (95% CI: 7–20 Å, see Table S4), which is in the lower range of previously reported values (approximately 10–40 Å)<sup>35–37,79</sup>. This analysis suggests that the pH effect influences diffusion along the aqueous pore pathway, via changes in porosity and tortuosity, as well as potentially affecting free-volume diffusion within the lipid matrix. In principle, both transport routes could be modulated by partial deprotonation of free fatty acids at neutral pH, as discussed above. However, given that low-molecular weight hydrophobic substances have been reported not to be affected by donor pH<sup>47</sup>, it is reasonable to propose that lipoidal free-volume diffusion is comparatively less influenced, whereas the aqueous pore pathway is more sensitive to pH dependent structural changes.

### Microbial conversion of niacinamide to nicotinic acid

While our results isolate the pH effect under controlled conditions, translation to practical topical use may be limited by the small volumes typically applied, although partial pH modulation may still be achievable with prolonged or occlusive applications such as patches or facemasks. In these cases, once applied to the skin, the composition of a formulation may be altered by skin-associated microbes. The human skin microbiome comprises a diverse community of commensal bacteria and fungi<sup>81,82</sup>, some of which are capable of metabolizing cosmetic ingredients. Examples include the fermentation of glycerol to lactic acid<sup>83</sup> and the hydrolysis of arbutin to hydroquinone<sup>84</sup>. For NIA, this is particularly relevant because many bacterial species carry the *pncA* gene, which encodes nicotinamidase, an enzyme that converts NIA into NA<sup>40,85,86</sup>. Since this metabolic pathway is absent in mammalian cells, the appearance of NA provides a specific indicator of microbial activity<sup>40</sup>. This distinction may be relevant for cosmetic scientists and formulators, as microbiome-driven transformations could influence the chemical profile and overall performance of topical NIA formulations.

In the extended pH switch experiment, a gradual decrease in NIA flux was observed when comparing fluxes between 8–12 h versus 32–36 h for pH 5.0, as well as between 20–24 h and 44–48 h for pH 7.4 (Fig. 3B). This trend was unexpected because prolonged aqueous exposure typically increases skin permeability<sup>38</sup>. A closer analysis of the HPLC–UV chromatograms, corresponding to the collected receptor samples during the prolonged permeation experiment, revealed the appearance of an additional peak after around 36 h, which increased steadily over time (Fig. 4A). This peak was identified as NA, consistent with microbial conversion of NIA. Low-level NA formation was also detectable in some of the 24 h permeation experiments conducted without  $\text{NaN}_3$ , although not consistently across all samples. Importantly, in the case when this peak was present,

the amount remained extremely small (<0.05% of the applied NIA). In contrast, NA was not detected when the 24 h permeation experiment was performed in the presence of 15 mM NaN<sub>3</sub>. Furthermore, bacterial cultures isolated from skin membranes converted NIA to NA only in the absence of NaN<sub>3</sub> (Fig. 4B). Together, these findings confirm that the minute decrease in flux during the later switch intervals, corresponding to time intervals 32–36 h and 44–48 h (Fig. 3B), compared with their respective earlier counterparts, originates from microbial metabolism of NIA. Although the conversion of NIA into NA observed in our experiments was small, it may be more pronounced under conditions that increase microbial activity, such as longer exposure times and conditions where higher microbial loads may be encountered. This is particularly relevant for real-world cosmetic applications, where skin-associated microbes are naturally present and where even low-level biotransformation may influence product performance.

## Conclusions

This work demonstrates that donor phase pH is a key determinant of skin permeability to niacinamide. A neutral donor pH promotes NIA permeability, which can be rationalized by partial deprotonation of free fatty acids that promotes defective microdomains of the SC lipid matrix, effectively enhancing niacinamide transdermal delivery. Comparable responses were observed in human skin and in the EpiDerm model, underscoring the value of reconstructed epidermal tissue models as viable tools for in vitro screening of transdermal delivery of cosmetic actives and drugs. Microbial conversion of niacinamide to nicotinic acid highlights the need to control microbial activity in long-duration studies. Overall, these findings establish pH modulation as a mild and reversible strategy for influencing niacinamide skin permeation, with implications for formulation design and dermal delivery of this substance.

## Data availability

Data supporting the findings of this study are available from the corresponding author on request.

Received: 20 December 2025; Accepted: 24 February 2026

Published online: 24 March 2026

## References

1. Michaels, A. S., Chandrasekaran, S. K. & Shaw, J. E. Drug permeation through human skin. Theory and in vitro experimental measurement. *AIChE J.* **21**, 985–996 (1975).
2. Scheuplein, R. J. & Blank, I. H. Permeability of the skin. *Physiol. Rev.* **51**, 702–747 (1971).
3. Bouwstra, J. A. et al. The skin barrier: An extraordinary interface with an exceptional lipid organization. *Prog. Lipid Res.* **92**, 101252. <https://doi.org/10.1016/j.plipres.2023.101252> (2023).
4. Sparr, E. et al. The stratum corneum barrier—From molecular scale to macroscopic properties. *Curr. Opin. Colloid Interface Sci.* **67**, 101725. <https://doi.org/10.1016/j.cocis.2023.101725> (2023).
5. Marques, C. et al. Mechanistic insights into the multiple functions of niacinamide: Therapeutic implications and cosmeceutical applications in functional skincare products. *Antioxidants* <https://doi.org/10.3390/antiox13040425> (2024).
6. Ong, R. R. & Goh, C. F. Niacinamide: A review on dermal delivery strategies and clinical evidence. *Drug Deliv. Transl. Res.* **14**, 3512–3548. <https://doi.org/10.1007/s13346-024-01593-y> (2024).
7. Jerajani, H. R., Mizoguchi, H., Li, J., Whittenbarger, D. J. & Marmor, M. J. The effects of a daily facial lotion containing vitamins B3 and E and provitamin B5 on the facial skin of Indian women: A randomized, double-blind trial. *Indian J. Dermatol. Venereol. Leprol.* **76**, 20–26. <https://doi.org/10.4103/0378-6323.58674> (2010).
8. Soma, Y. et al. Moisturizing effects of topical nicotinamide on atopic dry skin. *Int. J. Dermatol.* **44**, 197–202. <https://doi.org/10.1111/j.1365-4632.2004.02375.x> (2005).
9. Nisbet, S. et al. Cosmetic benefit of a biomimetic lamellar cream formulation on barrier function or the appearance of fine lines and wrinkles in randomized proof-of-concept clinical studies. *Int. J. Cosmet. Sci.* **41**, 1–11. <https://doi.org/10.1111/ics.12499> (2019).
10. Sjöberg, T. et al. Niacinamide and its impact on stratum corneum hydration and structure. *Sci. Rep.* **15**, 4953. <https://doi.org/10.1038/s41598-025-88899-0> (2025).
11. Gehring, W. Nicotinic acid/niacinamide and the skin. *J. Cosmet. Dermatol.* **3**, 88–93. <https://doi.org/10.1111/j.1473-2130.2004.00115.x> (2004).
12. Tan, C. Y. R. et al. Nicotinamide prevents UVB- and oxidative stress-induced photoaging in human primary keratinocytes. *J. Invest. Dermatol.* **142**, 1670–1681.e1612. <https://doi.org/10.1016/j.jid.2021.10.021> (2022).
13. Surjana, D., Halliday, G. M. & Damian, D. L. Role of nicotinamide in DNA damage, mutagenesis, and DNA repair. *J. Nucleic Acids.* **2010**, 157591. <https://doi.org/10.4061/2010/157591> (2010).
14. Bissett, D. L., Miyamoto, K., Sun, P., Li, J. & Berge, C. A. Topical niacinamide reduces yellowing, wrinkling, red blotchiness, and hyperpigmented spots in aging facial skin. *Int. J. Cosmet. Sci.* **26**, 231–238. <https://doi.org/10.1111/j.1467-2494.2004.00228.x> (2004).
15. Chiu, P.-C., Chan, C.-C., Lin, H.-M. & Chiu, H.-C. The clinical anti-aging effects of topical kinetin and niacinamide in Asians: A randomized, double-blind, placebo-controlled, split-face comparative trial. *J. Cosmet. Dermatol.* **6**, 243–249. <https://doi.org/10.1111/j.1473-2165.2007.00342.x> (2007).
16. Kawada, A., Konishi, N., Oiso, N., Kawara, S. & Date, A. Evaluation of anti-wrinkle effects of a novel cosmetic containing niacinamide. *J. Dermatol.* **35**, 637–642. <https://doi.org/10.1111/j.1346-8138.2008.00537.x> (2008).
17. Bogdanowicz, P. et al. Senomorphic activity of a combination of niacinamide and hyaluronic acid: Correlation with clinical improvement of skin aging. *Sci. Rep.* **14**, 16321. <https://doi.org/10.1038/s41598-024-66624-7> (2024).
18. Zhang, Y. et al. A comparison of the in vitro permeation of niacinamide in mammalian skin and in the Parallel Artificial Membrane Permeation Assay (PAMPA) model. *Int. J. Pharm.* **556**, 142–149. <https://doi.org/10.1016/j.ijpharm.2018.11.065> (2019).
19. Iliopoulos, F. et al. Topical delivery of niacinamide: Influence of neat solvents. *Int. J. Pharm.* **579**, 119137. <https://doi.org/10.1016/j.ijpharm.2020.119137> (2020).
20. Iliopoulos, F., Caspers, P. J., Puppels, G. J. & Lane, M. E. Franz cell diffusion testing and quantitative confocal Raman spectroscopy: In vitro-in vivo correlation. *Pharmaceutics* **12**, 887 (2020).
21. Zhang, W., Shi, X. & Zheng, S. Study on influencing factors of nicotinamide transdermal absorption in vitro and the establishment of an evaluation method. *Processes* **12**, 202 (2024).
22. Nowak, A. et al. Comparison of artificial hydrophilic and lipophilic membranes and human skin to evaluate niacinamide penetration in vitro. *Acta Pol. Pharm.* **77**, 271–279 (2020).

23. Brooks, S. G., Mahmoud, R. H., Lin, R. R., Fluhr, J. W. & Yosipovitch, G. The skin acid mantle: An update on skin pH. *J. Invest. Dermatol.* **145**, 509–521. <https://doi.org/10.1016/j.jid.2024.07.009> (2025).
24. Åberg, C., Wennerström, H. & Sparr, E. Transport processes in responding lipid membranes: A possible mechanism for the pH gradient in the stratum corneum. *Langmuir* **24**, 8061–8070 (2008).
25. Mojumdar, E. H. & Sparr, E. The effect of pH and salt on the molecular structure and dynamics of the skin. *Colloids Surf B Biointerfaces* **198**, 111476. <https://doi.org/10.1016/j.colsurfb.2020.111476> (2021).
26. Nováková, A. et al. Acidic pH is required for the multilamellar assembly of skin barrier lipids in vitro. *J. Invest. Dermatol.* **141**, 1915–1921.e1914. <https://doi.org/10.1016/j.jid.2021.02.014> (2021).
27. Bouwstra, J. A., Gooris, G. S., Dubbelaar, F. E. R., Ponec, M. & Weerheim, A. M. pH, cholesterol sulfate, and fatty acids affect the stratum corneum lipid organization. *J. Invest. Dermatol. Symp. Proc.* **3**, 69–74. <https://doi.org/10.1038/jidsymp.1998.17> (1998).
28. Yamamoto, T. & Yamamoto, Y. Electrical properties of the epidermal stratum corneum. *Med. Biol. Eng. Comput.* **14**, 151–158 (1976).
29. Björklund, S. et al. Skin membrane electrical impedance properties under the influence of a varying water gradient. *Biophys. J.* **104**, 2639–2650 (2013).
30. Morin, M., Runnsjö, A., Ruzgas, T., Engblom, J. & Björklund, S. Effects of storage conditions on permeability and electrical impedance properties of the skin barrier. *Int. J. Pharm.* **637**, 122891. <https://doi.org/10.1016/j.ijpharm.2023.122891> (2023).
31. Barbero, A. M. & Frasch, H. F. Effect of frozen human epidermis storage duration and cryoprotectant on barrier function using two model compounds. *Skin Pharmacol. Physiol.* **29**, 31–40. <https://doi.org/10.1159/000441038> (2016).
32. Dennerlein, K. et al. Studies on percutaneous penetration of chemicals—Impact of storage conditions for excised human skin. *Toxicol. In Vitro* **27**, 708–713. <https://doi.org/10.1016/j.tiv.2012.11.016> (2013).
33. Nielsen, J. B., Plasencia, I., Sørensen, J. A. & Bagatolli, L. A. Storage conditions of skin affect tissue structure and subsequent in vitro percutaneous penetration. *Skin Pharmacol. Physiol.* **24**, 93–102. <https://doi.org/10.1159/000322304> (2011).
34. Kempainen, B. W., Riley, R. T., Pace, J. G. & Hoerr, F. J. Effects of skin storage conditions and concentration of applied dose on [3H]T-2 toxin penetration through excised human and monkey skin. *Food Chem. Toxicol.* **24**, 221–227. [https://doi.org/10.1016/0278-6915\(86\)90232-2](https://doi.org/10.1016/0278-6915(86)90232-2) (1986).
35. Tang, H., Mitragotri, S., Blankschtein, D. & Langer, R. Theoretical description of transdermal transport of hydrophilic permeants: Application to low-frequency sonophoresis. *J. Pharm. Sci.* **90**, 545–568. [https://doi.org/10.1002/1520-6017\(200105\)90:5%3c545::aid-jps1012%3e3.0.co;2-h](https://doi.org/10.1002/1520-6017(200105)90:5%3c545::aid-jps1012%3e3.0.co;2-h) (2001).
36. Peck, K. D., Ghanem, A. H. & Higuchi, W. I. The effect of temperature upon the permeation of polar and ionic solutes through human epidermal membrane. *J. Pharm. Sci.* **84**, 975–982 (1995).
37. Tezel, A., Sens, A. & Mitragotri, S. Description of transdermal transport of hydrophilic solutes during low-frequency sonophoresis based on a modified porous pathway model. *J. Pharm. Sci.* **92**, 381–393. <https://doi.org/10.1002/jps.10299> (2003).
38. Björklund, S., Engblom, J., Thuresson, K. & Sparr, E. A water gradient can be used to regulate drug transport across skin. *J. Control Release* **143**, 191–200 (2010).
39. Jankovskaja, S. et al. Non-invasive skin sampling of tryptophan/kynurenine ratio in vitro towards a skin cancer biomarker. *Sci. Rep.* **11**, 678. <https://doi.org/10.1038/s41598-020-79903-w> (2021).
40. Huang, J. et al. The ratio of nicotinic acid to nicotinamide as a microbial biomarker for assessing cell therapy product sterility. *Mol. Ther. Methods Clin. Dev.* **25**, 410–424. <https://doi.org/10.1016/j.omtm.2022.04.006> (2022).
41. Sims, S. M., Higuchi, W. I. & Srinivasan, V. Skin alteration and convective solvent flow effects during iontophoresis: I. Neutral solute transport across human skin. *Int. J. Pharm.* **69**, 109–121. [https://doi.org/10.1016/0378-5173\(91\)90216-B](https://doi.org/10.1016/0378-5173(91)90216-B) (1991).
42. Kasting, G. B. & Bowman, L. A. DC electrical properties of frozen, excised human skin. *Pharm. Res.* **7**, 134–143 (1990).
43. Mitragotri, S. et al. Mathematical models of skin permeability: An overview. *Int. J. Pharm.* **418**, 115–129. <https://doi.org/10.1016/j.ijpharm.2011.02.023> (2011).
44. Potts, R. O. & Guy, R. H. Predicting skin permeability. *Pharm. Res.* **9**, 663–669 (1992).
45. Mitragotri, S. Modeling skin permeability to hydrophilic and hydrophobic solutes based on four permeation pathways. *J. Control Release* **86**, 69–92. [https://doi.org/10.1016/S0168-3659\(02\)00321-8](https://doi.org/10.1016/S0168-3659(02)00321-8) (2003).
46. Murthy, S. N., Sen, A., Zhao, Y.-L. & Hui, S. W. pH influences the postpulse permeability state of skin after electroporation. *J. Control Release* **93**, 49–57. <https://doi.org/10.1016/j.jconrel.2003.08.002> (2003).
47. Sznitowska, M., Janicki, S. & Baczek, A. Studies on the effect of pH on the lipoidal route of penetration across stratum corneum. *J. Control. Release* **76**, 327–335. [https://doi.org/10.1016/S0168-3659\(01\)00443-6](https://doi.org/10.1016/S0168-3659(01)00443-6) (2001).
48. Groen, D. et al. Disposition of ceramide in model lipid membranes determined by neutron diffraction. *Biophys. J.* **100**, 1481–1489. <https://doi.org/10.1016/j.bpj.2011.02.001> (2011).
49. Sagrafena, I. et al. Structure and function of skin barrier lipids: Effects of hydration and natural moisturizers in vitro. *Biophys. J.* **123**, 3951–3963. <https://doi.org/10.1016/j.bpj.2024.10.006> (2024).
50. Bouwstra, J. A., Gooris, G. S., Bras, W. & Downing, D. T. Lipid organization in pig stratum corneum. *J. Lipid Res.* **36**, 685–695 (1995).
51. Martin, M., Chantemargue, B. & Trouillas, P. Skin hydration by natural moisturizing factors, a story of H-bond networking. *J. Phys. Chem. B* **129**, 844–852. <https://doi.org/10.1021/acs.jpbc.4c05473> (2025).
52. Rerek, M. E., Van Wyck, D., Mendelsohn, R. & Moore, D. J. FTIR spectroscopic studies of lipid dynamics in phytosphingosine ceramide models of the stratum corneum lipid matrix. *Chem. Phys. Lipids* **134**, 51–58. <https://doi.org/10.1016/j.chemphyslip.2004.12.002> (2005).
53. Bouwstra, J. A. et al. Water distribution and related morphology in human stratum corneum at different hydration levels. *J. Invest. Dermatol.* **120**, 750–758 (2003).
54. Iwai, I. et al. The human skin barrier is organized as stacked bilayers of fully extended ceramides with cholesterol molecules associated with the ceramide sphingoid moiety. *J. Invest. Dermatol.* **132**, 2215–2225 (2012).
55. Björklund, S., Nowacka, A., Bouwstra, J. A., Sparr, E. & Topgaard, D. Characterization of Stratum Corneum molecular dynamics by natural-abundance <sup>13</sup>C solid-state NMR. *PLoS ONE* **8**, e61889. <https://doi.org/10.1371/journal.pone.0061889> (2013).
56. Alonso, A., Meirelles, N. C., Yushmanov, V. E. & Tabak, M. Water increases the fluidity of intercellular membranes of Stratum Corneum: Correlation with water permeability, elastic, and electrical resistance properties. *J. Invest. Dermatol.* **106**, 1058–1063. <https://doi.org/10.1111/1523-1747.ep12338682> (1996).
57. Silva, C. L. et al. Stratum Corneum hydration: Phase transformations and mobility in Stratum Corneum, extracted lipids and isolated corneocytes. *Biochim. Biophys. Acta (BBA)* **1768**, 2647–2659 (2007).
58. Johnson, M. E., Blankschtein, D. & Langer, R. Evaluation of solute permeation through the Stratum Corneum: Lateral bilayer diffusion as the primary transport mechanism. *J. Pharm. Sci.* **86**, 1162–1172 (1997).
59. Potts, R. & Francoeur, M. Lipid biophysics of water loss through the skin. *Proc. Natl. Acad. Sci. U. S. A.* **87**, 3871–3873 (1990).
60. Bodde, H. E., Van den Brink, I., Koerten, H. K. & De Haan, F. H. N. Visualization of in vitro percutaneous penetration of mercuric chloride; transport through intercellular space versus cellular uptake through desmosomes. *J. Control Release* **15**, 227–236 (1991).
61. White, S. H., Mirejovsky, D. & King, G. I. Structure of lamellar lipid domains and corneocyte envelopes of murine Stratum Corneum. An x-ray diffraction study. *Biochemistry* **27**, 3725–3732 (1988).
62. Forslind, B. A domain mosaic model of the skin barrier. *Acta. Derm. Venereol.* **74**, 1–6 (1994).
63. Bouwstra, J. A., Helder, R. W. J. & El Ghalbzouri, A. Human skin equivalents: Impaired barrier function in relation to the lipid and protein properties of the stratum corneum. *Adv. Drug Deliv. Rev.* **175**, 113802. <https://doi.org/10.1016/j.addr.2021.05.012> (2021).

64. Spector, A. A. Fatty acid binding to plasma albumin. *J. Lipid Res.* **16**, 165–179. [https://doi.org/10.1016/s0022-2275\(20\)36723-7](https://doi.org/10.1016/s0022-2275(20)36723-7) (1975).
65. Villalain, J. & Gómez-Fernández, J. C. Fourier transform infrared spectroscopic study of mixtures of palmitic acid with dipalmitoylphosphatidylcholine using isotopic substitution. *Chem. Phys. Lipids* **62**, 19–29. [https://doi.org/10.1016/0009-3084\(92\)90050-Y](https://doi.org/10.1016/0009-3084(92)90050-Y) (1992).
66. Cistola, D. P., Hamilton, J. A., Jackson, D. & Small, D. M. Ionization and phase behavior of fatty acids in water: Application of the Gibbs phase rule. *Biochemistry* **27**, 1881–1888. <https://doi.org/10.1021/bi00406a013> (1988).
67. Hamilton, J. A. & Cistola, D. P. Transfer of oleic acid between albumin and phospholipid vesicles. *Proc. Natl. Acad. Sci. U. S. A.* **83**, 82–86. <https://doi.org/10.1073/pnas.83.1.82> (1986).
68. Lieckfeldt, R., Villalain, J., Gómez-Fernández, J. C. & Lee, G. Apparent pKa of the fatty acids within ordered mixtures of model human stratum corneum lipids. *Pharm. Res.* **12**, 1614–1617. <https://doi.org/10.1023/a:1016280714593> (1995).
69. Morin, M. et al. Skin hydration dynamics investigated by electrical impedance techniques in vivo and in vitro. *Sci. Rep.* **10**, 17218. <https://doi.org/10.1038/s41598-020-73684-y> (2020).
70. Kalia, Y. N., Piro, F. & Guy, R. H. Homogeneous transport in a heterogeneous membrane: Water diffusion across human stratum corneum in vivo. *Biophys. J.* **71**, 2692–2700. [https://doi.org/10.1016/s0006-3495\(96\)79460-2](https://doi.org/10.1016/s0006-3495(96)79460-2) (1996).
71. White, E. A., Orazem, M. E. & Bunge, A. L. Characterization of damaged skin by impedance spectroscopy: Mechanical damage. *Pharm. Res.* **30**, 2036–2049. <https://doi.org/10.1007/s11095-013-1052-1> (2013).
72. Hernández, A. R. et al. Algae extract-based nanoemulsions for photoprotection against UVB radiation: An electrical impedance spectroscopy study. *Sci. Rep.* **15**, 1911. <https://doi.org/10.1038/s41598-025-85604-z> (2025).
73. Hernández, A. R., Vallejo, B., Ruzgas, T. & Björklund, S. The effect of UVB irradiation and oxidative stress on the skin barrier—A new method to evaluate sun protection factor based on electrical impedance spectroscopy. *Sensors* **19**, 2376 (2019).
74. Potts, R. O., Guy, R. H. & Francoeur, M. L. Routes of ionic permeability through mammalian skin. *Solid State Ionics* **53–56**, 165–169. [https://doi.org/10.1016/0167-2738\(92\)90378-3](https://doi.org/10.1016/0167-2738(92)90378-3) (1992).
75. Albér, C. et al. Effects of water gradients and use of urea on skin ultrastructure evaluated by confocal Raman microspectroscopy. *Biochim. Biophys. Acta (BBA) Biomembranes* **1828**, 2470–2478. <https://doi.org/10.1016/j.bbamem.2013.06.011> (2013).
76. Warner, R. R., Stone, K. J. & Boissy, Y. L. Hydration disrupts human stratum corneum ultrastructure. *J. Invest. Dermatol.* **120**, 275–284 (2003).
77. Warner, R. R. et al. Water disrupts stratum corneum lipid lamellae: Damage is similar to surfactants. *J. Invest. Dermatol.* **113**, 960–966 (1999).
78. Kontturi, K. & Murtomaki, L. Impedance spectroscopy in human skin. A refined model. *Pharm. Res.* **11**, 1355–1357 (1994).
79. Peck, K. D., Ghanem, A.-H. & Higuchi, W. I. Hindered diffusion of polar molecules through and effective pore radii estimates of intact and ethanol treated human epidermal membrane. *Pharm. Res.* **11**, 1306–1314 (1994).
80. Kushner, J. IV, Blankschtein, D. & Langer, R. Evaluation of the porosity, the tortuosity, and the hindrance factor for the transdermal delivery of hydrophilic permeants in the context of the aqueous pore pathway hypothesis using dual-radiolabeled permeability experiments. *J. Pharm. Sci.* **96**, 3263–3282. <https://doi.org/10.1002/jps.20955> (2007).
81. Grice, E. A. & Segre, J. A. The skin microbiome. *Nat. Rev. Microbiol.* **9**, 244–253. <https://doi.org/10.1038/nrmicro2537> (2011).
82. Byrd, A. L., Belkaid, Y. & Segre, J. A. The human skin microbiome. *Nat. Rev. Microbiol.* **16**, 143–155. <https://doi.org/10.1038/nrmi.2017.157> (2018).
83. Salgaonkar, N. et al. Glycerol fermentation by skin bacteria generates lactic acid and upregulates the expression levels of genes associated with the skin barrier function. *Exp. Dermatol.* **31**, 1364–1372. <https://doi.org/10.1111/exd.14604> (2022).
84. Bang, S.-H., Han, S.-J. & Kim, D.-H. Hydrolysis of arbutin to hydroquinone by human skin bacteria and its effect on antioxidant activity. *J. Cosmet. Dermatol.* **7**, 189–193. <https://doi.org/10.1111/j.1473-2165.2008.00387.x> (2008).
85. Feng, S., Guo, L., Wang, H., Yang, S. & Liu, H. Bacterial PncA improves diet-induced NAFLD in mice by enabling the transition from nicotinamide to nicotinic acid. *Commun. Biol.* **6**, 235. <https://doi.org/10.1038/s42003-023-04613-8> (2023).
86. Wang, P. et al. Microecology in vitro model replicates the human skin microbiome interactions. *Nat. Commun.* **16**, 3085. <https://doi.org/10.1038/s41467-025-58377-2> (2025).

## Acknowledgements

We gratefully acknowledge the financial support from the Swedish Knowledge Foundation (grant number: 20220031). We thank master students Xandra Huynh and Andebrhan Fsayeh at Malmö University for their assistance with solubility measurements and permeation experiments. We also acknowledge Volodymyr Kuzmenko (CellInk), Lene Visdal-Johnsen (Oriflame), and Sandra Smiljanic (Oriflame) for fruitful discussions during this project.

## Author contributions

Thomas Sjöberg: Investigation; Methodology; Data Curation; Formal Analysis; Writing Original Draft; Writing—Review & Editing. Silvia Letasiova: Project Administration; Resources. Skaidre Jankovskaja: Methodology; Writing—Review & Editing. Nina Hrapovic: Project Administration; Resources. Christina Österlund: Project Administration; Resources. Emelie J. Nilsson: Supervision; Writing—Review & Editing. Johan Engblom: Supervision; Writing—Review & Editing. Peter Spegel: Methodology; Writing—Review & Editing. Sebastian Björklund: Conceptualization; Methodology; Data Curation; Formal Analysis; Project Administration; Supervision; Funding Acquisition; Writing—Original Draft; Writing Review & Editing.

## Funding

Open access funding provided by Malmö University. This work was financially supported by the Swedish Knowledge Foundation (grant number: 20220031).

## Declarations

## Competing interests

The authors declare no competing interests.

## Additional information

**Supplementary Information** The online version contains supplementary material available at <https://doi.org/10.1038/s41598-026-41992-4>.

**Correspondence** and requests for materials should be addressed to S.B.

**Reprints and permissions information** is available at [www.nature.com/reprints](http://www.nature.com/reprints).

**Publisher's note** Springer Nature remains neutral with regard to jurisdictional claims in published maps and institutional affiliations.

**Open Access** This article is licensed under a Creative Commons Attribution 4.0 International License, which permits use, sharing, adaptation, distribution and reproduction in any medium or format, as long as you give appropriate credit to the original author(s) and the source, provide a link to the Creative Commons licence, and indicate if changes were made. The images or other third party material in this article are included in the article's Creative Commons licence, unless indicated otherwise in a credit line to the material. If material is not included in the article's Creative Commons licence and your intended use is not permitted by statutory regulation or exceeds the permitted use, you will need to obtain permission directly from the copyright holder. To view a copy of this licence, visit <http://creativecommons.org/licenses/by/4.0/>.

© The Author(s) 2026